Global Observations of Acetyl Peroxynitrate (PAN) in the Remote Troposphere

Young Ro Lee[1], L. Gregory Huey[1†], David J. Tanner[1], James M. Roberts[2], Yuhang Wang[1], Paul O. Wennberg[3], John D. Crounse[3], Hannah Allen[3], Eric C. Apel[4], Alan J. Hills[4], Rebecca S. Hornbrook[4], James W. Elkins[5], Eric Hintsa[5,7], Fred Moore[5,7], Samuel R. Hall[4], Kirk Ullmann[4], Kathryn McKain[5], Colm Sweeney[5], Thomas B. Ryerson[2], Jeff Peischl[2,6], Chelsea R. Thompson[2,6], Ilann Bourgeois[2,6], Eric Ray[2,6], Paul A. Newman[8] and Sarah Strode[8,9]

[1]School of Earth and Atmospheric Sciences, Georgia Institute of Technology, Atlanta, GA, USA, [2]NOAA Chemical Sciences Laboratory, Boulder, CO, USA, [3]Division of Geological and Planetary Sciences, California Institute of Technology, Pasadena, CA, USA, [4]Atmospheric Chemistry Observations & Modeling, NSF National Center for Atmospheric Research, Boulder, CO, USA, [5]NOAA Global Monitoring Laboratory, Boulder, CO, USA, [6]Cooperative Institute for Research in Environmental Sciences, University of Colorado, Boulder, CO, USA, [7]Department of Earth System Science, University of California, Irvine, CA, USA, [8]NASA Goddard Space Flight Center, MD, USA, [9]Morgan State University, GESTAR-II, Baltimore, MD, USA

[†]*Correspondence to*: L. G. Huey (greg.huey@eas.gatech.edu)

Abstract

We present global airborne observations of acetyl peroxynitrate ($CH_3C(O)OONO_2$, PAN) in the remote troposphere from the Atmospheric Tomography (ATom) campaign. These observations show that biomass burning is the dominant source of PAN in the Southern Hemisphere. In the Northern Hemisphere, anthropogenic emissions from Asia and Europe, also contribute significantly to PAN over the Pacific and Atlantic oceans. Model simulations underestimate PAN in the lower troposphere, in part, due to the underestimation of local production driven by acetaldehyde oxidation and β_{NO_2} (the ratio of acetyl peroxy (PA) radicals reacting with NO_2 relative to other pathways). The significant impacts of biomass burning evident in the ATom PAN observations suggest that improving model treatment of plume transport and the conversion of NO_x to PAN in biomass burning plumes is a viable focus for better simulating PAN. Global observations of PAN provide a benchmark for the evaluation of satellite observations and model simulations of PAN.

Plain Language Summary

We report the global airborne observations of acetyl peroxynitrate (PAN) from the Atmospheric Tomography (ATom) campaign. Biomass burning is the dominant source of PAN over the remote oceans in the Southern Hemisphere. Anthropogenic emissions from Asia and Europe significantly contribute to PAN levels over the Pacific and Atlantic oceans, alongside biomass burning. Model simulations underestimates PAN in the lower oceanic troposphere, partly due to an underestimation in local production driven by acetaldehyde. Our observations show strong evidence of the persistent of biomass burning influence on PAN throughout the remote troposphere, particularly over the Southern Hemispheric oceans. This work provides a valuable data set to improve understanding the global distribution of PAN.

Key Points

- Global airborne observations of PAN over the remote troposphere during the ATom campaign are presented.
- Biomass burning emissions are the dominant source of PAN over the Southern Hemispheric oceans, while in the Northern Hemisphere, anthropogenic emissions from Asia and Europe significantly contribute to the remote tropospheric PAN levels alongside biomass burning.
- Model simulations underestimate the local production of PAN in the lower oceanic troposphere, driven by acetaldehyde, as well as the impact of biomass burning on PAN levels throughout the remote troposphere.

1 Introduction

Acetyl peroxynitrate (PAN) is an important reservoir for nitrogen oxides (NO_x). In many regions of the troposphere, PAN is the primary form of reactive nitrogen (NO_y) (Roberts et al., 2007). PAN can undergo long-range transport as it is insoluble and quite stable at cold temperatures (lifetime of PAN, τ_{PAN}, up to a month in the upper troposphere) (Singh & Hanst, 1981; Talukdar et al., 1995; Frenzel et al., 2000). Transport and subsequent thermolysis of PAN to release NO_x may be essential for photochemical ozone (O_3) production in the remote troposphere (Kasibhatla et al., 1993; Moxim et al., 1996; Fischer et al., 2014).

Despite significant advances in understanding the distribution of PAN on a global scale, large uncertainties persist in the remote troposphere. Previous studies attributed pollution episodes in remote marine environments, where PAN is a major component of NO_y, to continental transport from urban areas, biomass burning and lightning-NO_x emissions (e.g., Wahner et al., 1994; Singh et al., 1996, 2006 and 2009; Blake et al., 1999; Roberts et al., 2004; Fischer et al., 2014). However, the global impact of these sources, particularly in remote regions like the Southern Hemisphere oceans, remains poorly characterized. Observations in these regions are scarce but are critical for diagnosing the key factors controlling the global distribution of PAN including changing impacts of continental emissions, transport, and the atmospheric chemistry of pollutants transported to the remote troposphere (Roberts et al., 2007). Recent studies from the NASA Atmospheric Tomography (ATom) campaign, considered here, emphasize gaps in understanding remote tropospheric composition. These include missing sources of primary PAN precursors such as acetaldehyde and NO_x over remote oceans (Wang et al., 2019; Shah et al., 2023), and the significant contribution of biomass burning to the global distribution of O_3, peroxides and particles (Bourgeois et al., 2021; Allen et al., 2022; Schill et al., 2020). Observations of PAN in the remote troposphere, in combination with satellite observations and model simulations, are also critical for addressing gaps in our understanding.

In this work, we present global-scale airborne PAN observations with high temporal resolution and extensive spatial coverage from the ATom campaign (Thompson et al., 2021). These observations provide "background" levels of PAN and its precursors in regions previously lacking extensive measurements, achieved through near-continuous vertical sampling and flight strategies designed for an unbiased assessment of the remote troposphere. We report mixing ratios of PAN over the remote Pacific and Atlantic Oceans in all seasons. We examine the distribution of PAN in the remote troposphere by a combined analysis of observations and model simulations including emission tracer measurements, back-trajectory analyses, and tagged emission tracer simulations. A diagnostic evaluation of both PAN and its precursor simulations from a Chemical Transport Model

(CTM) was performed using observations and kinetic calculations highly constrained by measured parameters. Lastly, we utilize measurements of biomass burning tracers and simulated biomass burning contributions to carbon monoxide (CO) to investigate the impact of biomass burning on the relationship between observed and simulated PAN.

2 Methods

A comprehensive suite of chemical, physical and meteorological measurements was conducted aboard the NASA DC-8 research aircraft during the four ATom deployments from 28 July 2016 (ATom–1) to 21 May 2018 (ATom–4). Each deployment, lasting for approximately one month in each season, followed near-identical flight plans as described by Figure S1a and Thompson et al. (2021). Instrumentation details are provided in Table S1. Data were merged to a 10-second time base or the Trace Organic Gas Analyzer (TOGA) sampling interval (35 seconds every two minutes) and filtered to exclude data obtained over continental regions. The geographical boundaries used to filter the data are illustrated along with the flight tracks in Figure S1b. We removed data with stratospheric influence defined as when O_3 and O_3/CO were greater than 100 ppbv and 1 ppbv $ppbv^{-1}$, respectively, at altitudes greater than 6 km. A marked decrease in CFC-113 provided an additional proxy for stratospheric influence, employing the 25th-percentile value (70–72 pptv) across each deployment as a cut-off. This effectively excluded data obtained at the edges of stratospheric-influenced samples that often have O_3 levels lower than 100 ppbv (Figure S2). In addition, data in which the photolysis rate of J_{NO2} was below its 10th percentile (solar zenith angle ~ 90°) were excluded in kinetic calculations.

Alongside extensive observations, the ATom dataset includes model products and trajectory calculations. To investigate the potential impact of transpacific transport on the observed trace gas composition, 10-day back trajectory ensembles, which were initialized at each minute along the ATom flight tracks, were utilized (Ray, 2021). Data points whose back trajectories intersected the boundaries of East Asia, as shown in Figure S1b, were identified as having "East Asian influence (EAI)." As transpacific transport is a complex process unlikely to be fully represented using a single method, we assessed systematic differences in measured chemical tracers such as carbon monoxide (CO), hydrogen cyanide (HCN), propionyl peroxynitrate (PPN) and PAN, for data with and without EAI. This analysis is facilitated by incorporating the Goddard Earth Observing System Version 5 (GEOS-5) simulations of tagged-CO concentrations, which well predicted the distribution, source, and episodic enhancements of CO during ATom–1 (Strode et al., 2018; Newman & Pawson, 2021). Our method to identify EAI is described in section 4 of the supporting information (SI) using data from the 6 October 2017 research flight, which sampled both East Asian transport and Southern Hemisphere biomass burning events.

A key focus of the ATom measurements is to provide observational constraints to evaluate model-simulated remote tropospheric composition, previously hindered by a lack of relevant observations in such regions. For this purpose, we utilized outputs from the Global Modeling Initiative (GMI)–CTM (Strode et al., 2021). The performance of different CTMs with various meteorological and chemical schemes has been discussed elsewhere (e.g., Travis et al., 2020; Shah et al., 2022). Briefly, the GMI-CTM provides trace gas mixing ratios with a spatial resolution of 1° latitude × 1.25° longitude × 72 vertical levels and a temporal resolution of 15 minutes, interpolated to the ATom flight tracks (Strode et al., 2021). The same criteria used to filter observational data were applied to the

model outputs. For a diagnostic analysis of model simulated PAN, we compared the model outputs with the observed hydrocarbon and radical precursors of PAN, as well as the estimated acetyl peroxy (PA) radical concentrations. The impact of observation-model discrepancies in these variables on PAN simulations are investigated by comparing the simulated PAN to the observed data and steady state (SS) calculation for PAN when temperatures were above 290 K, the median value observed in the lower troposphere (<2 km) during ATom. This allows identification of data in which the SS estimation for PAN is most valid. The details in the calculations and estimated uncertainties are described in the SI.

3 Results

3.1 PAN mixing ratios

Figure 1a illustrates the vertical profiles of median PAN mixing ratios in 1-km altitude bins over the tropics (0°–20°), mid-latitudes (20°–60°), and polar regions (60°–90°) in the Northern Hemisphere (NH) and Southern Hemisphere (SH) in each season. In the NH lower troposphere (<2 km), PAN mixing ratios were generally higher in the extratropics than in the tropics. A notable exception was observed in July–August, where the highest PAN levels (median of 20 pptv) were measured in the tropical lower troposphere. This coincided with the highest PAN production rate (P_{PAN}, median of 13 pptv hr^{-1}) and the shortest τ_{PAN} ~ 0.8 hours, suggesting efficient local production of PAN over the tropical oceans in this case. The latitudinal differences in vertical PAN mixing ratios are particularly noticeable in April–May, when PAN in the extratropics was higher than that in the tropics at all altitudes. Springtime enhancements of PAN in the NH remote extratropics have been attributed to the transport of continental outflow when photochemical production of PAN is efficient and its thermal decomposition is relatively slow (Penkett & Brice, 1986; Bottenheim et al., 1994).

On average, PAN in the NH increased with altitude from the low to mid-troposphere but decreased above 8 km, in part due to loss by photolysis in the upper troposphere. In the SH, PAN also leveled off in the upper troposphere. Increasing PAN levels with altitude were associated with the increasing PAN lifetime and concurrent enhancements of combustion tracers such as CO and HCN. The contribution of local P_{PAN}, which was dominated by acetaldehyde oxidation, to this vertical distribution was minimal (Figure S5). Net P_{PAN} (P_{PAN}-loss rate of PAN, L_{PAN}) were below 1ppt hr^{-1} in the free troposphere over both the Pacific and Atlantic Oceans. In July–August, high PAN levels persisted above 8 km in all latitude bins. The elevated PAN was coincident with HCN up to 680 pptv and a high probability of convective influence (a factor of 3.5 greater than the annual median in the upper troposphere), which was estimated based on the back trajectories and satellite detection of cloud locations as used by Allen et al. (2022) to examine global peroxide distributions during ATom. This suggests that transport of biomass burning plumes coupled with convection is critical to explain the NH PAN distribution in summer.

Unlike the complicated latitudinal distribution of PAN in the NH, PAN in the SH increased almost linearly at a rate of roughly 0.7 pptv per degree latitude from the South Pole to the tropics on average. In this work, the latitudinal gradient of PAN in the SH is attributed to increasing biomass burning impacts from Africa, South America, and Australia over the SH tropics. Median PAN mixing ratios in the mid- and upper troposphere were significantly higher in austral winter (July–August) and spring (September–October), the dry seasons with frequent burning events (Andreae et al., 2012; Paton-Walsh et al., 2022). The highest median value of PAN was observed at

6–8 km during austral spring. This springtime PAN maximum in the SH agrees with previous studies including recent satellite observations (Fischer et al., 2014; Pope et al., 2016). On the basis of strong correlations of PAN with biomass burning tracers (section 3.2), we attribute the austral spring PAN maximum as well as most of the SH PAN variations to biomass burning.

Figures 1b and 1c shows median PAN mixing ratios and PAN to NO_y ratios in 4-degree latitude and 1-km altitude bins, respectively. Elevated levels of PAN and its contribution to NO_y were observed throughout the NH extratropical troposphere. PAN remained a major component of NO_y in both the NH and SH extratropical free troposphere but was depleted in the tropical lower troposphere. This is consistent with previous remote surface measurements of PAN (e.g., Rudolph et al., 1987; Müller & Rudolph, 1992; Roberts et al., 2007 and references therein). Our work attributes low PAN levels in the tropics to a net negative PAN production rate (median of P-L = -0.6 pptv hr^{-1}) driven by thermal decomposition. Over the tropical Pacific Ocean, the patterns in latitude-altitude cross sections of PAN were consistent with those in L_{PAN} (Figures 1b and S5d). Despite the similarity of L_{PAN} over the Atlantic Ocean to the global trend, PAN was more than 30% of NO_y throughout the tropical Atlantic troposphere. This is consistent with strong enhancements of HCN (>200 pptv) and CO (>100 ppbv) throughout the subtropical Atlantic troposphere (Figure S6a-b), indicating the influence of biomass burning on PAN and its contribution to NO_y in the regions. Consequently, PAN and PAN/NO_y over the Atlantic Ocean were more consistent across latitudes and altitudes in contrast to the significant variations observed between the NH and SH Pacific Oceans.

3.2 Sources of PAN

We investigate the influence of continental sources on PAN in the remote mid- and upper troposphere (altitudes > 4 km), where PAN has a relatively long lifetime (up to three weeks). We utilize chemical tracers of specific pollution sources and the categorizations of data based on back-trajectory analysis. Namely, we used high temporal resolution measurements of HCN and CO from biomass burning and general combustion emissions, respectively. (Holzinger et al., 1999). PPN was used as a photochemical tracer of anthropogenic emissions (Roberts et al., 2007; Lee et al., 2021). Note that measurements of PPN were not available for July–August (ATom-1).

Figure 2 illustrates the seasonal trends of PAN along with those of chemical tracers using box plots. The marked increases in PAN during the SH fire seasons (September–October) were consistent with those of HCN and CO for both the SH Pacific and Atlantic Oceans (Figure 2a-b). Despite the wide geographic coverage of the data, a strong correlation (r^2 > 0.7) between PAN and HCN was notable over the SH Oceans (Figure 2c), highlighting the significant contribution of biomass burning to PAN in these regions. This chemical tracer analysis was further facilitated by TOGA measurements of two anthropogenic tracers, C_2Cl_4 and CH_2Cl_2, and a biomass burning tracer CH_3CN (Apel et al., 2015; Roozitalab et al., 2024). The analysis using TOGA measurements agreed well with analysis that used the faster time response measurements. The correlations of PAN, CO, and PPN with the biomass burning tracers (HCN and CH_3CN) were significantly higher than those with the anthropogenic tracers measured by TOGA. For this reason, this work suggests that biomass burning is the primary contributor to PAN and pollutant distribution in the SH.

The seasonal trends of PAN were more comparable to those of HCN than those of CO for both the NH Pacific and Atlantic Oceans (Figure 2d–e). PAN showed moderate correlations with HCN over the NH Pacific and Atlantic Oceans (r^2 = 0.5 and 0.3, respectively), indicating a notable contribution of biomass burning transport to PAN in the NH (Figure 2f). Over the NH Pacific Ocean, the correlations of PAN and CO with C_2Cl_4 and CH_2Cl_2 were similar to those with HCN, suggesting that anthropogenic emissions are also important contributors to PAN over this region. PPN, derived largely from anthropogenic precursors, showed moderate correlations with anthropogenic (r^2 of 0.4 and 0.3 with C_2Cl_4 and CH_2Cl_2, respectively) and burning (r^2 > 0.3 with CH_3CN) tracers only over the NH Pacific Ocean and SH Oceans, respectively. While PAN and PPN showed a negligible relationship with anthropogenic tracers including CO over the NH Atlantic Ocean, increasing values of PAN mixing ratios were often coincident with elevations in the observed propane mixing ratios and the fractional contribution of CO from European non-biomass burning source ($CO_{non\text{-}BB\ EU}$) in GEOS-5 simulations in the extratropical regions (latitude > 30°) (Figure S7). The highest levels of PAN and propane were observed up to 400 pptv and 1.3 ppbv, respectively, along with greater than 60% combined contribution of $CO_{non\text{-}BB\ EU}$ and CO from Asian non-biomass burning sources ($CO_{non\text{-}BB\ Asia}$) in GEOS-5. Consequently, this suggests that enhancements of PAN in the NH Atlantic extratropical regions may be more associated with anthropogenic emissions from Europe and Asia than from North America.

The observed relationships between PAN and chemical tracers point out the important contribution of both anthropogenic and biomass burning emissions to PAN levels over the NH Pacific Ocean. An important anthropogenic pollution source in the NH Pacific Ocean is transpacific transport from East Asia (Wang et al., 2003; Roberts et al., 2004), with its strongest influence in spring (Stohl et al., 2002; Liu et al., 2005). Figure 3 shows cumulative distribution functions (CDFs) of PAN and related tracers with and without EAI, determined from the back trajectories, using mid- and upper tropospheric data for the NH. On the basis of the CDFs in Figure 2g, data with EAI contained elevated levels of PAN and tracers, with mixing ratios of PAN, CO, HCN, and PPN being 2.7, 1.3, 1.3 and 2.3 times higher, respectively, compared to those without EAI. The elevated levels of CO are consistent with a 26% higher fractional contribution of $CO_{non\text{-}BB\ Asia}$ to the total CO in GEOS-5 simulations. Similar systematic differences in PAN levels have been reported by previous observations. For example, airborne measurements during ITCT 2K2 (Intercontinental Transport and Chemical Transformation 2002) campaign observed up to 650 pptv of PAN accompanied with CO mixing ratios above 150 ppbv (Roberts et al., 2004; Nowak et al., 2004). In accordance with these findings, Figure 2h illustrates data with EAI contains higher levels of both PAN and CO, along with larger slopes and r^2 for linear regressions between PAN and CO, as well as the higher fractional contribution of $CO_{non\text{-}BB\ Asia}$. The median mixing ratios of PAN and CO with significant EAI peaked in spring with a value ~70% greater than the annual median, whereas those without EAI peaked in summer. This seasonal trend of PAN also agrees with the stronger impacts of transpacific transport on pollution over the Pacific Ocean during springtime (Jaffe et al., 1999; Zhang et al., 2008). In summary, this work suggests that PAN over the NH is largely influenced by complicated sources such as biomass burning and anthropogenic emissions including transpacific transport, whereas PAN over the SH can be largely accounted for by biomass burning emissions.

3.3 Diagnostic evaluation of modeled PAN using observations

Figure 3a illustrates the probability distribution function (PDF) of observed and modeled acetaldehyde and β_{NO_2}, where β_{NO_2} represents the ratio of PA reacting with NO_2 to the total reacting with NO, NO_2, HO_2 and RO_2. When PAN approaches steady state (SS) due to rapid thermal decomposition over the remote lower troposphere, its concentration depends linearly on the production rate of PA, primarily driven by the oxidation of acetaldehyde by the OH radical (e.g., Figure S5), but inversely on the product of the thermal decomposition rate and $1/\beta_{NO_2} - 1$ (Sillman et al., 1990). On average, the model underestimated both acetaldehyde and β_{NO_2} when using steady-state NO_2 (β_{SS-NO_2}). In this section, NO_2 from pseudo-steady state (SS-NO_2) calculations is used due to potential measurement interferences from thermally labile species and larger discrepancy between the observed NO_2 and the estimated values based on SS calculations and model simulations at higher altitudes (Nault et al., 2015; Shah et al., 2023). The model underestimation of acetaldehyde was persistent across altitudes, in accordance with the findings of Wang et al. (2019) during ATom 1–2. In contrast, the model underestimated $\beta_{\mathrm{NO_2}}$ more significantly in the lower troposphere, which is consistent with the underestimation in modeled NO_x using both GMI and GEOS-Chem without photolysis of particulate nitrate at altitudes below 6 km, as discussed by Shah et al. (2023).

Figure 3b compares PA concentrations directly from the 3-D model output and those derived from SS calculations using modeled and observed constraints. To be consistent with SS calculations for PAN (Figure 3c), only data with temperatures >290 K were included. On average, PA concentrations from both the model output and SS calculations using modeled PAN precursors were approximately 90% lower than the estimated values based on observations and equations in the SI (SE1-2). Improved agreement between the modeled and observed PA was found when the relative difference between modeled and observed acetaldehyde was lower.

The remote lower tropospheric conditions observed during ATom facilitate the diagnosis of the model-simulated PAN by comparison with SS calculations of PAN. In these conditions, the short τ_{PAN}, persistent acetaldehyde levels and limited perturbation from transport improve validity of the SS calculations (Cleary et al., 2007 , SI section 4 and Figures S8 and 9). Figure 3c illustrates that observed PAN is in better agreement with the SS estimation than the 3-D model. The agreement between the modeled and observed PAN improves when $\beta_{\mathrm{NO_2}}$ and PA from the 3-D model and observations are consistent. Consequently, this suggests that model simulations of PAN in the remote lower troposphere can be improved by addressing the model bias in acetaldehyde and $\beta_{\mathrm{NO_2}}$.

Biomass burning emissions had significant impact on the remote tropospheric PAN distribution during ATom. In particular, strong linear relationships between PAN and HCN were notable in the SH. Figure S10 illustrates this linear relationship across altitude bins for both the NH and SH observations. To investigate the impact of biomass burning on the observation-model discrepancies in PAN, we focused on the percent difference of PAN between observations and GMI model simulations in the SH due to the relatively simple emission source characteristics dominated by biomass burning. Figure 3d illustrates the percent difference of PAN increased with fractional contribution of CO from global biomass burning in GEOS-5, which is consistent with increasing percent difference of PAN with observed HCN levels (Figure S10). The increase in the percent difference of PAN was found while CO from GEOS-5 agrees with both CO from GMI and observations within 30%. For this reason, we suggest that model simulations of the global PAN distribution will depend on accurate treatment of chemical evolution in biomass burning plumes as well as emissions and transport. Measurements of PAN in the SH, presented

in this work, may be useful to evaluate the simulated influence of biomass burning on PAN due to the dominant contribution of biomass burning to PAN distributions in these regions.

4 Discussion

This work presents observations of the remote tropospheric PAN distribution. Biomass burning has a large and persistent impact on PAN across the globe, and is a dominant source of PAN in the SH. The significant global effects of biomass burning on PAN are likely due to the injection of its precursors in biomass burning plumes that are often transported at higher altitudes, where thermolysis is slower and wind speeds are higher (e.g., Ke et al., 2021). Global satellite observations have attributed a significant portion of upper tropospheric and lower stratospheric PAN to biomass burning with pyro-convective transport, which is in accordance with our findings. (Moore & Remedios, 2010; Tereszchuk et al., 2013; Pope et al., 2016). Notably, the agreement between modeled and observed vertical distributions of PAN and CO was greatly improved for North American boreal regions with the implementation of a new fire plume injection scheme based on satellite data into GEOS-Chem (Zhu et al., 2018).

Efficient PAN production is commonly observed in biomass burning plumes (Alvarado et al., 2010; Liu et al., 2016; Wolfe et al., 2022), but simulating this process using a CTM has proven challenging due to complex factors such as emissions, plume injection, mixing, and photochemistry (Andreae, 2019; Liu et al., 2016; Wang et al., 2021). Based on our recent PAN measurements during the 2019 NASA/NOAA FIREX-AQ (Fire Influence on Regional to Global Environments of Air Quality) campaign, PAN often constitutes 40–50% of NO_y a few hours downwind of biomass burning, which is consistent with findings from previous observations (Alvarado et al., 2010; Liu et al., 2016). The relatively consistent contribution of observed PAN to NO_y may result from a combined effect of these factors. While a detailed assessment of PAN chemistry is crucial for understanding the chemical evolution of biomass burning emissions, assigning ~40% of biomass burning NO_x emissions to PAN seems reasonable for a 3-D CTM focusing on the global distribution of PAN (e.g., Alvarado et al., 2010; Fischer et al., 2014). However, different fire types (e.g., wildfire and prescribed burning) exhibit markedly different conversion rates of NO_x to PAN (e.g., Liu et al., 2016, 2017). This suggests that implementation of different conversion rates to attribute initial NO_x emissions to PAN based on fire types could be tested as a more effective modeling strategy. Recently, retrieval products from the TROPOspheric Monitoring Instrument (TROPOMI) were used by Jin et al. (2021) to estimate global biomass burning NO_x emission factors and lifetimes for different fuel types. Their satellite-based NO_2 analysis illustrated decreasing NO_x lifetime with fire emissions due to changing chemical regimes (from NO_x limited to saturated regimes). However, the ability to understand the impacts of PAN on the evolution of NO_x using an exponentially modified Gaussian analysis on TROPOMI NO_2 columns was limited, highlighting the complexity of NO_y processing in fire plumes. Consequently, our work suggests that the model treatments of plume transport and conversion of biomass burning NO_x emissions to PAN are an important focus for reliably simulating the impacts of biomass burning on global PAN distributions.

5 Conclusion

This work reports global-scale airborne observations of remote tropospheric PAN during the ATom campaign. PAN concentrations over the NH oceans were impacted by a complex mix of sources such as

anthropogenic emissions, transpacific transport from East Asia, and biomass burning. Biomass burning has a dominant and persistent impact on PAN in the SH. Our diagnostic evaluation of modeled PAN and its precursors based on observations suggests the GMI model should account for the underestimations of acetaldehyde and β_{NO_2} to improve PAN simulations in the lower troposphere. In addition, we suggest that accurate treatment of biomass burning should be a focus for model simulations of PAN in the remote troposphere. The remote tropospheric PAN observations in this work provide a valuable data set for model evaluations and the analyses and evaluation of satellite observations.

Figures

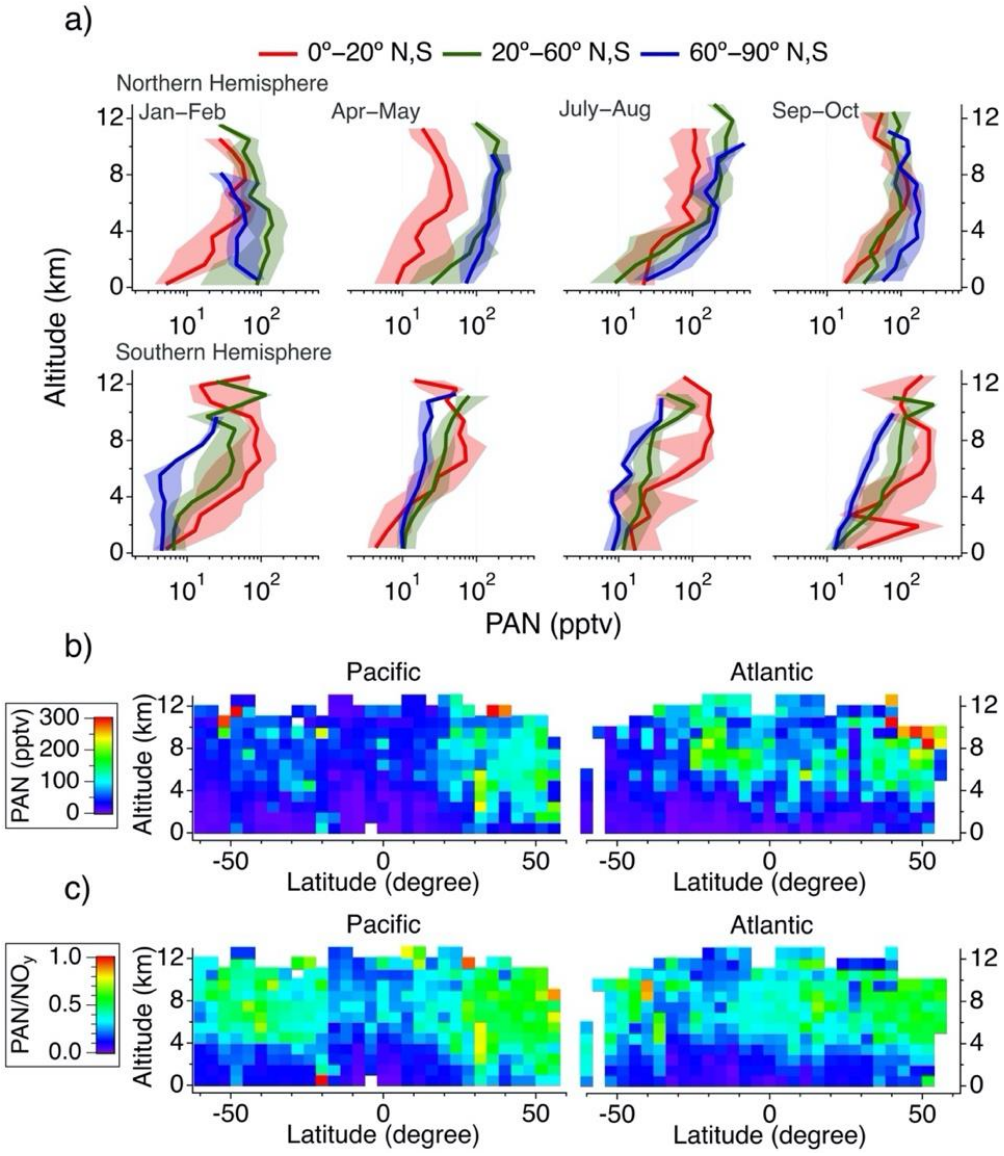

Figure 1. (a) Vertical profiles of median PAN mixing ratios in 1-km altitude bins over the tropics (red), mid-latitudes (green), and polar regions (blue) of the NH (top panels) and SH (bottom panels), with shaded areas indicating 25th and 75th percentiles. Altitude plots of (b) PAN and (c) PAN to NO_y ratios as a function of latitude.

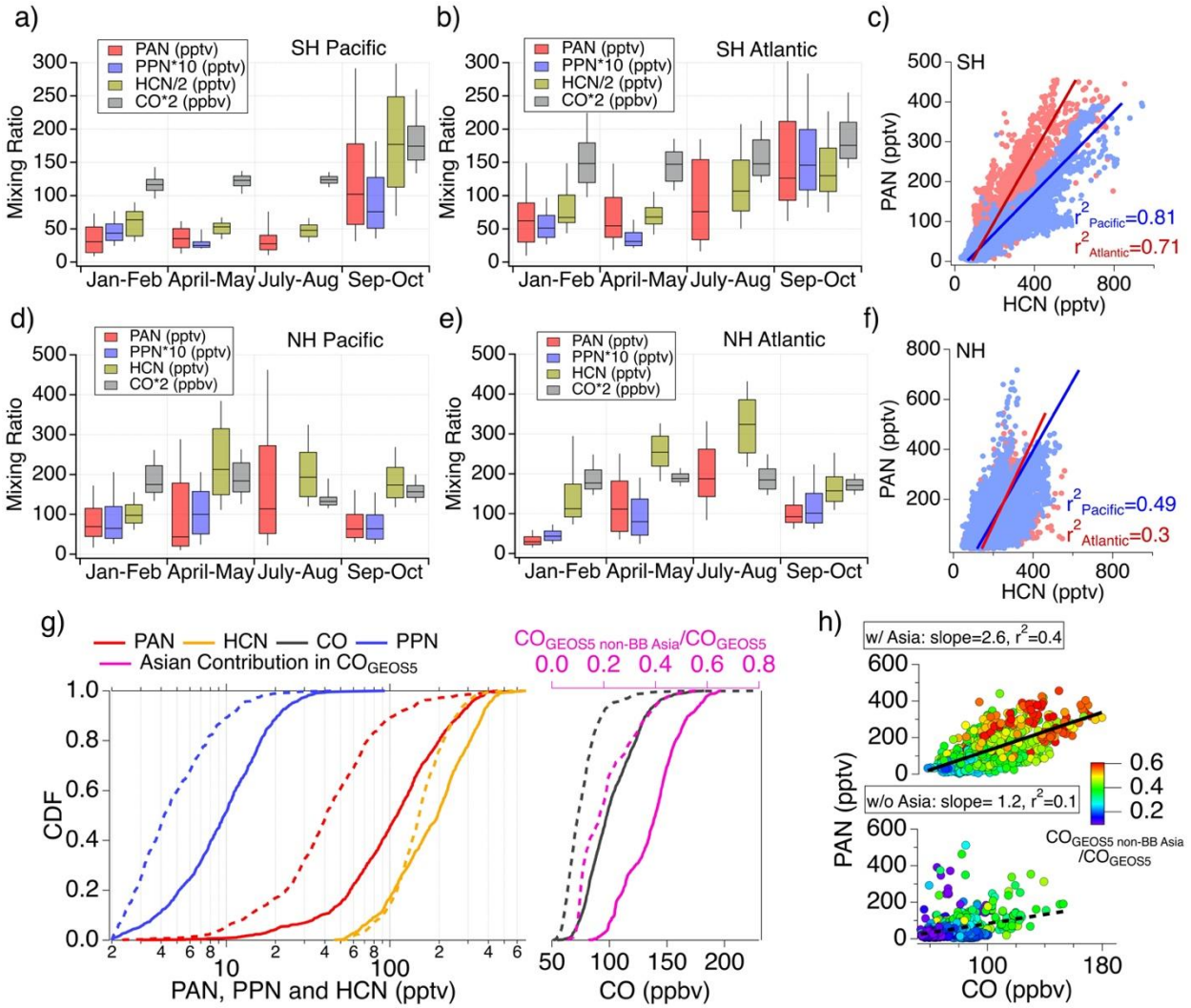

Figure 2. Box and whisker plots of selected tracers observed over the SH (a) Pacific and (b) Atlantic, and (c) scatter plot of observed PAN versus HCN for the SH oceans in all four seasons. Box and whisker plots of selected tracers observed over the NH (d) Pacific and (e) Atlantic, and (f) scatter plot of observed PAN versus HCN for the NH oceans in all four seasons. (g) Cumulative Distribution Functions (CDFs) of observed PAN, PPN, HCN and CO and the fractional contributions of modeled CO from non-biomass burning Asian sources in GEOS-5 ($CO_{GEOS5\ non\text{-}BB\ Asia}$) over the NH Pacific Ocean. Solid and dashed lines represent data with and without East Asian influence, respectively. (h) Scatter plots of observed PAN versus CO (top) with and (bottom) without East Asian influence colored using the ratios of $CO_{GEOS5\ non\text{-}BB\ Asia}$ to the total CO in GEOS-5.

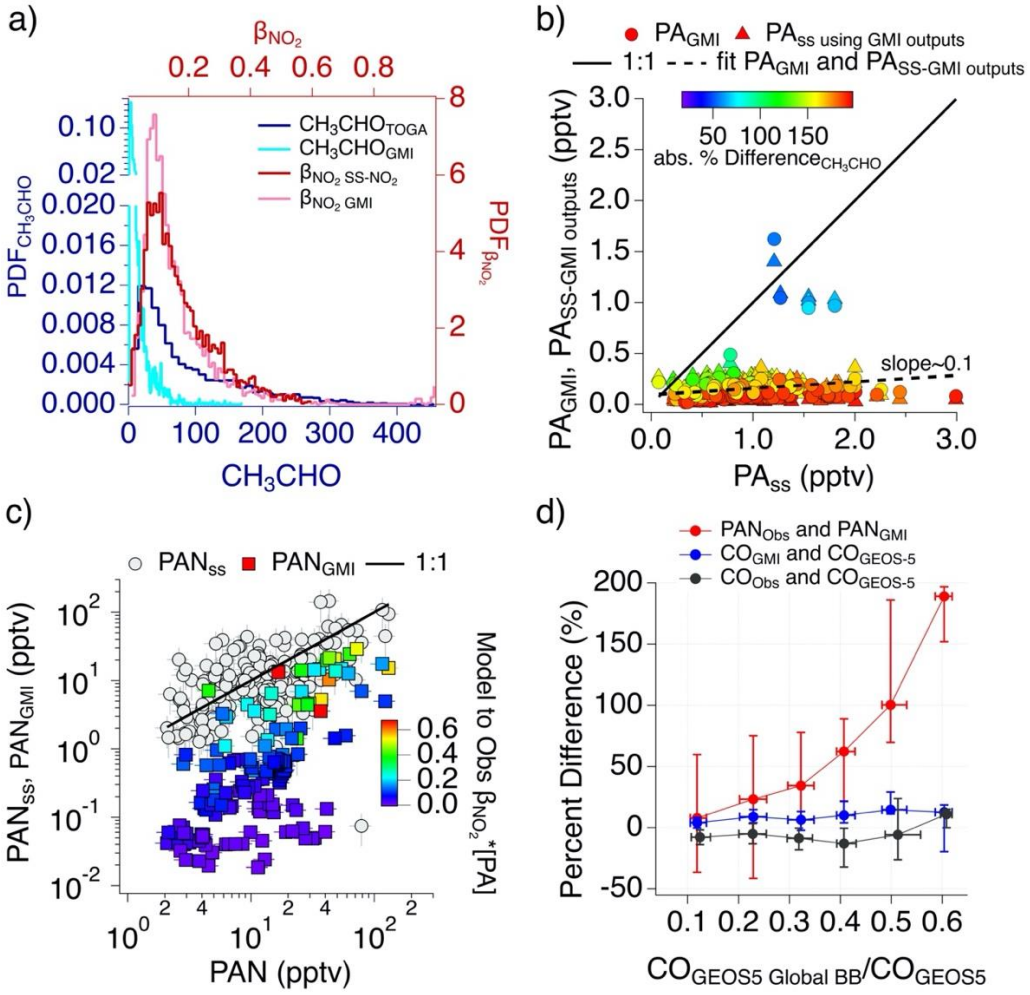

Figure 3. (a) Probability distribution functions (PDFs) of observed and modeled CH_3CHO and β_{NO_2}. (b) Scatter plots of PA concentrations from both the model outputs (PA_{GMI}) and steady state (SS) calculations using modeled PA precursors ($PA_{SS\text{-}GMI}$) against SS calculations using observations. Data points are color-coded based on the absolute percent difference between modeled and observed CH_3CHO. (c) Scatter plots of PAN from SS calculations (PAN_{SS}) and model simulations (PAN_{GMI}) versus observed PAN. (d) Percent differences between observed and GMI-modeled PAN (red), GMI-modeled and GEOS5 modeled CO (blue), and observed and GEOS5-modeled CO (gray), which are illustrated as a function of fractional contribution of CO from global biomass burning ($CO_{GEOS5\ Global\ BB}$) to total CO in GEOS5 in the SH.

Acknowledgements

The PAN observations and analysis were supported by NASA grants NNX15AT90G and 80NSSC23K0826**.** This material is based upon work supported by the NSF National Center for Atmospheric Research, which is a major facility sponsored by the U.S. National Science Foundation under Cooperative Agreement No. 1852977. The GMI CTM was supported by the NASA Modeling, Analysis and Prediction (MAP) program. The NASA High-End Computing Program (HEC) provided computational resources through the NASA Center for Climate Simulation (NCCS) for the GMI CTM simulation.

Data Availability

The data used in this work is available from the ATom campaign archive at https://doi.org/10.3334/ORNLDAAC/1925 (Wofsey et al., 2021). The GMI modelling results for the ATom campaign are available at https://doi.org/10.3334/ORNLDAAC/1897 (Strode et al., 2021).

References

Allen H. M., Crounse, J. D., Kim, M. J., Teng, A. P., Ray, E. A., McKain, K., et al. (2022). H_2O_2 and CH_3OOH (MHP) in the Remote Atmosphere: 1. Global Distribution and Regional Influences. *Journal of Geophysical Research: Atmospheres*, 127, e2021JD035701. https://doi.org/10.1029/2021JD035701

Alvarado, M. J., Logan, J. A., Mao, J., Apel, E., Riemer, D., & Blake, D., et al. (2010). Nitrogen oxides and PAN in plumes from boreal fires during ARCTAS-B and their impact on ozone: an integrated analysis of aircraft and satellite observations. *Atmospheric Chemistry and Physics*, 10, 9739–9760. https://doi.org/10.5194/acp-10-9739-2010

Andreae, M. O. (2019). Emission of trace gases and aerosols from biomass burning - an updated assessment. *Atmospheric Chemistry and Physics*, 19, 8523–8546. https://doi.org/10.5194/acp-19-8523-2019

Andreae, M. O., Artaxo, P., Beck, V., Bela, M., Freitas, S., Gerbig, C., et al. (2012). Carbon monoxide and related trace gases and aerosols over the Amazon Basin during the wet and dry seasons. *Atmospheric Chemistry and Physics*, 12, 6041–6065. https://doi.org/10.5194/acp-12-6041-2012

Apel, E. C., Hornbrook, R. S., Hills, A. J., Blake, N. J., Barth, M. C., Weinheimer, A., et al. (2015). Upper tropospheric ozone production from lightning NO_x-impacted convection: Smoke ingestion case study from the DC3 campaign. *Journal of Geophysical Research: Atmospheres*, 102, 2505–2523. https://doi.org/10.1002/2014JD022121

Blake, N. J., Blake, D. R., Wingenter, O. W., Sive, B. C., McKenzie, L. M., Lopez, J. P., et al. (1999). Influence of southern hemispheric biomass burning on midtropospheric distributions of nonmethane hydrocarbons and selected halocarbons over the remote South Pacific. *Journal of Geophysical Research: Atmopsheres*, 104, 16213–16232. https://doi.org/10.1029/1999JD900067

Bottenheim, J. W., Sirois, A., Brice, K. A., & Gallant, A. J. (1994). Five years of continuous observations of PAN and ozone at a rural location in eastern Canada. *Journal of Geophysical Research: Atmopsheres*, 99, 5333–5352. https://doi.org/10.1029/93JD02716

Bourgeois, I., Peischl, J., Neuman, J. A., Brown, S. S., Thompson, C. R., Aikin, K. C., et al. (2021). Large contribution of biomass burning emissions to ozone throughout the global remote troposphere. *Proceedings of the National Academy of Sciences of the USA*, 118 (52), e2109628118. https://doi.org/10.1073/pnas.2109628118

Wang, S., Coggon, M. M., Gkatzelis, G. I., Warneke, C., Bourgeois, I., Ryerson, T., et al. (2021). Chemical tomography in a fresh wildland fire plume: A large eddy simulation (LES) study. *Journal of Geophysical Research: Atmospheres*, 126, e2021JD035203. https://doi.org/10.1029/2021JD035203

Cleary, P. A., Wooldridge, P. J., Millet, D. B., McKay, M., Goldstein, A. H., & Cohen, R. C. (2007). Observations of total peroxy nitrates and aldehydes: measurement interpretation and inference of OH radical concentrations, *Atmospheric Chemistry and Physics*, 7, 1947–1960. https://doi.org/10.5194/acp-7-1947-2007

Fischer, E. V., Jacob, D. J., Yantosca, R. M., Sulprizio, M. P., Millet, D. B., Mao, J. F., et al. (2014). Atmospheric peroxyacetyl nitrate (PAN): A global budget and source attribution. *Atmospheric Chemistry and Physics*, 14, 2679–2698. https://doi.org/10.5194/acp-14-2679-2014

Jaffe, D., Anderson, T., Covert, D., Kotchenruther, R., Trost, B., Danielson, J., et al. (1999). Transport of Asian Air Pollution to North America. *Geophysical Research Letters*, 26, 6, 711–714. https://doi.org/10.1029/1999GL900100

Jin, X., Zhu, Q., & Cohen, R. C. (2021). Direct estimates of biomass burning NO_x emissions and lifetimes using daily observations from TROPOMI. *Atmospheric Chemistry and Physics*, 21, 15569–15587. https://doi.org/10.5194/acp-21-15569-2021

Kasibhatla, P. S., Levy, H., & Moxim, W. J. (1993). Global NO_x, HNO_3, PAN, and NO_y distributions from fossil fuel combustion emissions: A model study. *Journal of Geophysical Research: Atmospheres*, 98(D4), 7165–7180. https://doi.org/10.1029/92jd02845

Ke, Z., Wang, Y., Zou, Y., Song, Y., & Liu, Y. (2021). Global Wildfire Plume-Rise Data Set and Parameterizations for Climate Model Applications. *Journal of Geophysical Research: Atmospheres*, 126, e2020JD033085. https://doi.org/10.1029/2020JD033085

Liu, J., Mauzerall, D. L., & Horowitz, L. W. (2005). Analysis of seasonal and interannual variability in transpacific transport. *Journal of Geophysical Research: Atmospheres*, 110, D04302. https://doi.org/10.1029/2004JD005207

Liu, X., Zhang, Y., Huey, L. G., Yokelson, R. J., Selimovic, V., Simpson, I. J., et al. (2017). Airborne measurements of western U. S. wildfire emissions: Comparison with prescribed burning and air quality implications. *Journal of Geophysical Research: Atmospheres*, 122, 6108–6129. https://doi.org/10.1002/2016JD026315

Liu, X., Zhang, Y., Huey, L. G., Yokelson, R. J., Wang, Y., Jimenez, J. L., et al. (2016). Agricultural fires in the southeastern U.S. during SEAC4RS: Emissions of trace gases and particles and evolution of ozone, reactive nitrogen, and organic aerosol. *Journal of Geophysical Research: Atmospheres*, 121, 7383–7414. https://doi.org/10.1002/2016JD025040

Moore, D. P., & Remedios, J. J. (2010). Seasonality of Peroxyacetyl nitrate (PAN) in the upper troposphere and lower stratosphere using the MIPAS-E instrument, *Atmospheric Chemistry and Physics*, 10(13), 6117–6128. https://doi.org/10.5194/acp-10-6117-2010

Moxim, W. J., Levy H., & Kasibhatla, P. S. (1996). Simulated global tropospheric PAN: Its transport and impact on NO_x. *Journal of Geophysical Research: Atmospheres*, 101(D7), 12621–12638. https://doi.org/10.1029/96jd00338.

Müller, K. P., & Rudolph, J. (1992). Measurements of Peroxyacetylnitrate in the Marine Boundary Layer over the Atlantic. *Journal of Atmospheric Chemistry*, 15, 361–367. https://doi.org/10.1007/BF00115405

Nault, B. A., Garland, C., Pusede, S. E., Wooldridge, P. J., Ullmann, K., Hall, S. R., et al. (2015). Measurements of $CH_3O_2NO_2$ in the upper troposphere, *Atmospheric Measurement Techniques*, 8, 987–997. https://doi.org/10.5194/amt-8-987-2015

Newman, P. A., & Pawson, S. (2021). ATom: GEOS-5 Derived Meteorological Conditions and Tagged Tracers Along Flight Tracks. ORNL Distributed Active Archive Center. https://doi.org/10.3334/ORNLDAAC/1876

406 Nowak, J. B., Parrish, D. D., Neuman, J. A., Holloway, J. S., Cooper, O. R., Ryerson, T. B., et al. (2004). Gas-phase
407 chemical characteristics of Asian emission plumes observed during ITCT 2K2 over the eastern North Pacific Ocean.
408 *Journal of Geophysical Research: Atmospheres*, 119, DS23S19. https://doi.org/10.1029/2003JD004488
409 Paton-Walsh, C., Emmerson, K. M., Garland, R. M., Keywood, M., Hoelzemann, J. J., Huneeus, N., et al. (2022). Key
410 challenges for tropospheric chemistry in the Southern Hemisphere. *Elementa Science of the Anthropocene*, 10: 1.
411 https://doi.org/10.1525/elementa.2021.00050
412 Penkett, S. A., & Brice, K. A. (1986). The spring maximum in photo-oxidants in the Northern Hemisphere troposphere.
413 *Nature*, 319, 655–657. https://doi.org/10.1038/319655a0
414 Pope, R. J., Richards, N. A. D., Chipperfield, M. P., Moore, D. P., Monks, S. A., Arnold, S. R., et al. (2016).
415 Intercomparison and evaluation of satellite peroxyacetyl nitrate observations in the upper troposphere-lower
416 stratosphere. *Atmospheric Chemistry and Physics*, 16, 13541–13559. https://doi.org/10.5194/acp-16-13541-2016
417 Ray, E. A. (2021). ATom: Back Trajectories and Influences of Air Parcels Along Flight Track 2016-2018. ORNL
418 Distributed Active Archive Center. https://doi.org/10.3334.ORNLDAAC/1889
419 Roberts, J. M. (2007). PAN and related compounds. In Volatile organic compounds in the atmosphere (pp. 221–268).
420 Blackwell Publishing Ltd. https://doi.org/10.1002/9780470988657.ch6
421 Roberts, J. M., Flocke, F., Chen, G., de Gouw, J., Holloway, J. S., Hubler, G., et al. (2004). Measurement of
422 peroxycarboxylic nitric anhydrides (PANs) during the ITCT 2K2 aircraft intensive experiment. *Journal of*
423 *Geophysical Research: Atmospheres*, 109, D23S21. https://doi.org/10.1029/2004JD004960
424 Roozitalab, B., Emmons, L. K., Hornbrook, R. S., Kinnison, D. E., Fernandez, R. P., Li, Q., et al. (2024). Measurements
425 and Modeling of the Interhemispheric Differences of Atmospheric Chlorinated Very Short-Lived Substances.
426 *Journal of Geophysical Research: Atmospheres*, 129, e2023JD039518. https://doi.org/10.1029/2023JD039518
427 Rudolph, J., Rudolph-Vierkorn, B., & Meixner, F. X. (1987). Large-Scale Distribution of Peroxyacetylnitrate Results
428 From the STRATOZ III Flights. *Journal of Geophysical Research: Atmospheres*, 92, D6, 6653–6661.
429 https://doi.org/10.1029/JD092iD06p06653
430 Schill, G. P., Froyd, K. D., Brian, H., Kupc, A., Williamson, C., Brock, C. A., et al. (2020). Widespread biomass
431 burning smoke throughout the remote troposphere. *Nature Geoscience*, 13, 422–427. https://doi.org/
432 10.1038/s41561-020-0586-1
433 Shah, V., Jacob, D. J., Dang, R., Lamsal, L. N., Strode, S. A., Steenrod, S. D., et al. (2023). Nitrogen oxides in the free
434 troposphere: implications for tropospheric oxidants and the interpretation of satellite NO_2 measurements.
435 *Atmospheric Chemistry and Physics*, 23, 1227–1257. https://doi.org/10.5194/acp-23-1227-2023
436 Sillman, S., Logan, J. A., & Wofsy, S. C. (1990). The Sensitivity of Ozone to Nitrogen Oxides and Hydrocarbons in
437 Regional Ozone Episodes. *Journal of Geophysical Research: Atmospheres*, 95, D2. 1837–1851.
438 https://doi.org/10.1029/JD095iD02p01837
439 Singh H. B., & Hanst P. L. (1981). Peroxyacetyl Nitrate (PAN) in the unpolluted atmosphere: an important reservoir for
440 nitrogen oxides. *Geophysical Research Letters*, 8, 941–944. https://doi.org./10.1029/GL008i008p00941

441 Singh, H. B., Brune, W. H., Crawford, J. H., Flocke, F. & Jacob, D. J. (2009). Chemistry and transport of pollution over
442 the Gulf of Mexico and the Pacific: spring 2006 INTEX-B campaign overview and first results, *Atmospheric*
443 *Chemistry and Physics*, 9, 2301–2318. https://doi.org/10.5194/acp-9-2301-2009
444 Singh, H. B., Brune, W. H., Crawford, J. H., Jacob, D. J., & Russell P. B. (2006). Overview of the summer 2004
445 Intercontinental Chemical Transport Experiment–North America (INTEX-A). *Journal of Geophysical Research:*
446 *Atmospheres*, 111, D24S01. https://doi.org/10.1029/2006JD007905
447 Stohl, A., Eckhardt, S., Forster, C., James, P., & Spichtinger, N. (2002). On the pathways and timescales of
448 intercontinental air pollution transport. *Journal of Geophysical Research: Atmospheres*, 107, D23, 4684.
449 https://doi.org/10.1029/2001JD001396
450 Strode, S. A., Liu, J., Lait, L., Commane, R., Daube, B., Wofsy, S., et al. (2018). Forecasting carbon monoxide on a
451 global scale for the ATom-1 aircraft mission: insights from airborne and satellite observations and modeling.
452 *Atmospheric Chemistry and Physics*, 18, 10955–10971. https://doi.org/10.5194/acp-18-10955-2018
453 Strode, S.A., Steenrod, S. D., Nicely, J. M., Liu, J., Damon, M. R., & Strahan, S. E. (2021). ATom: Global Modeling
454 Initiative (GMI) Chemical Transport Model (CTM) Output. ORNL Distributed Active Archive Center.
455 https://doi.org/10.3334/ORNLDAAC/1897
456 Talukdar, R. K., Burkholder, J. B., Schmoltner, A.-M., Roberts, J. M., Wilson, R. R., & Ravishankara, A. R. (1995).
457 Investigation of the loss processes for peroxyacetyl nitrate in the atmosphere: UV photolysis and reaction with OH.
458 *Journal of Geophysical Research: Atmospheres*, 100(D7), 14163. https://doi.org/10.1029/95jd00545
459 Tereszchuk, K. A., Moore, D. P., Harrison, J. J., Boone, C. D., Park, M., & Remedios, J. J., et al. (2013). Observations
460 of peroxyacetyl nitrate (PAN) in the upper troposphere by the Atmospheric Chemistry Experiment-Fourier
461 Transform Spectrometer (ACE-FTS). *Atmospheric Chemisry and Physics*, 13, 5601–5613.
462 https://doi.org/10.5194/acp-13-5601-2013
463 Thompson, C. R., Wofsy, S. C., Prather, M. J., Newman, P. A., Hanisco, T. F., Ryerson, T. B., et al. (2021). The NASA
464 Atmospheric Tomography (ATom) Mission - Imaging the Chemistry of the Global Atmosphere. *Bulletin of the*
465 *American Meteorological Society*, 103, 3, E761–E790. https://doi.org/10.1175/BAMS-D-20-0315.1
466 Travis, K. R., Heald, C. L., Allen, H. M., Apel, E. C., Arnold, S. R., Blake, D. R., et al. (2020). Constraining remote
467 oxidation capacity with ATom observations. *Atmospheric Chemistry and Physics*, 20, 7753–7781.
468 https://doi.org/10.5194/acp-20-7753-2020
469 Wahner A., Rohrer, F., Ehhalt, D. H., Atlas, E., & Ridley, B. (1994). Global measurements of photochemically active
470 compounds. *Environmental Science Research: Global Atmospheric-Biospheric Chemistry*, 48, Plenum Press, New
471 York.
472 Wang, S., Coggon, M. M., Gkatzelis, G. I., Warneke, C., Bourgeois, I., Ryerson, T., et al. (2021). Chemical
473 Tomography in a Fresh Wildland Fire Plume: A Large Eddy Simulation (LES) Study. *Journal of Geophysical*
474 *Research:Atmospheres*, 126, e2021JD035203. https://doi.org/10.1029/2021JD035203
475 Wang, S., Hornbrook, R. S., Hills, A., Emmons, L. K., Tilmes, S., Lamarque, J.-F., et al. (2019). Atmospheric
476 acetaldehyde: Importance of air-sea exchange and a missing source in the remote troposphere. *Geophysical*
477 *Research Letters*, 46, 5601–5613. https://doi.org/10.1029/2019GL082034

Wang, Y., Shim, C., Blake, N., Blake, D., Choi, Y., Ridley, B., et al. (2003). Intercontinental transport of pollution manifested in the variability and seasonal trend of springtime O_3 at northern middle and high latitudes. *Journal of Geophysical Research: Atmospheres*, 108, D21, 4683. https://doi.org/10.1029/2003JD003592

Wofsy, S.C., et al. (2021). ATom: Merged Atmospheric Chemistry, Trace Gases, and Aerosols, Version 2. ORNL DAAC, Oak Ridge, Tennessee, USA. https://doi.org/10.3334/ORNLDAAC/1925

Wolfe, G. M., Hanisco, T. F., Arkinson, H. L., Blake, D. R., Wisthaler, A., Mikoviny, T., et al. (2022). Photochemical evolution of the 2013 California Rim Fire: synergistic impacts of reactive hydrocarbons and enhanced oxidants. *Atmospheric Chemistry and Physics*, 22, 4253–4275. https://doi.org/10.5194/acp-22-4253-2022

Zhang, L., Jacob, D. J., Boersma, K. F., Jaffe, D. A., Olson, J. R., Bowman, K. W., et al. (2008). Transpacific transport of ozone pollution and the effect of recent Asian emission increases on air quality in North America: an integrated analysis using satellite, aircraft, ozonesonde, and surface observations. *Atmospheric Chemistry and Physics*, 8, 6117–6136. https://doi.org/10.5194/acp-18-6117-2008

Zhu, L., Martin, M. V., Gatti, L. V., Kahn, R., Hecobian, A., & Fischer, E. V. (2018). Development and implementation of a new biomass burning emissions injection height scheme (BBEIH v1.0) for the GEOS-Chem model (v9-01-01). *Geoscientific Model Development*, 11, 4103–4116. https://doi.org/10.5194/gmd-11-4103-2018